Supporting Information

Handedness Matters: Parallel Alignment of Electric and Magnetic Transition Dipole Moments in Chiral Additives Boosts Oxygen Evolution Reaction

Julia Portela-Pino,[1,2] Isilda Amorim,[3] Stefano Chiussi,[4] Laura M. Salonen,[5,3] Ani Ozcelik,[1] Daniel Aranda,[6,7] Joonas Uusitalo,[8] Ángeles Peña-Gallego,[2] Fabrizio Santoro,[9]* Yury V. Kolen'ko,[3]* José Lorenzo Alonso-Gómez[1]*

Section 1

Enantiomeric Resolution of 2,2'-Dibromo-9,9'-spirobifluorene (Br_2-SBF)

The enantiomeric resolution of Br_2-SBF was carried out through HPLC using a chiral stationary phase (CSP), using a preparative Chiralpak IB-N column (30 mm x 250 mm) supplied by Daicel Chemical Industries.

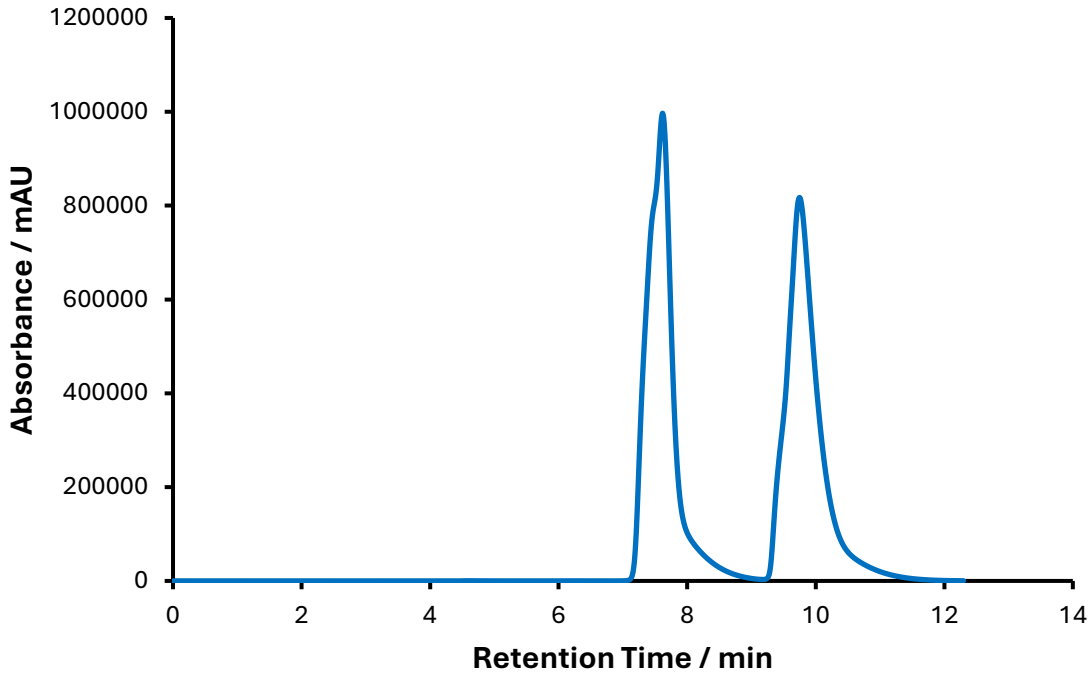

Figure S1: Conditions: Chiral stationary phase Chiralpak IB N-5 30 mm x 250 mm, mobile phase hexane/dichloromethane (DCM) (95:5); flow rate: 30 mL/min; column temperature: 25 ºC; detection wavelength: 270 nm; injection volume: 450 µL. Retention time first peak: 7,6 min. Retention time second peak: 9,7 min.

Synthesis of (*M,M*/*P,P*)-2 and (*M,M,M*/*P,P,P*)-1 from Enantiopure Br_2-SBF

The systems under study, (*M,M*/*P,P*)**-2** and (*M,M,M*/*P,P,P*)**-1** have been reported earlier as diastereomeric mixtures that were resolved obtaining all optically active stereoisomers. In this work we performed the stereospecific synthesis of the homochiral isomers (the same absolute configuration for all the chiral axes in the system) by using enantiopure Br_2-SBF as starting material. Additionally, the control of temperature and reagents addition rate enabled access to dimeric and trimeric cyclic oligomers from the same synthetic method. Comparison of Nuclear Magnetic Resonance (^{1}H NMR) and electron circular dichroism (CD) spectra of (*M,M*)**-2**, (*P,P*)**-2**, (M,*M,M*)**-1**, and (*P,P,P*)**-1** confirmed their structures and optical purities. [1,2]

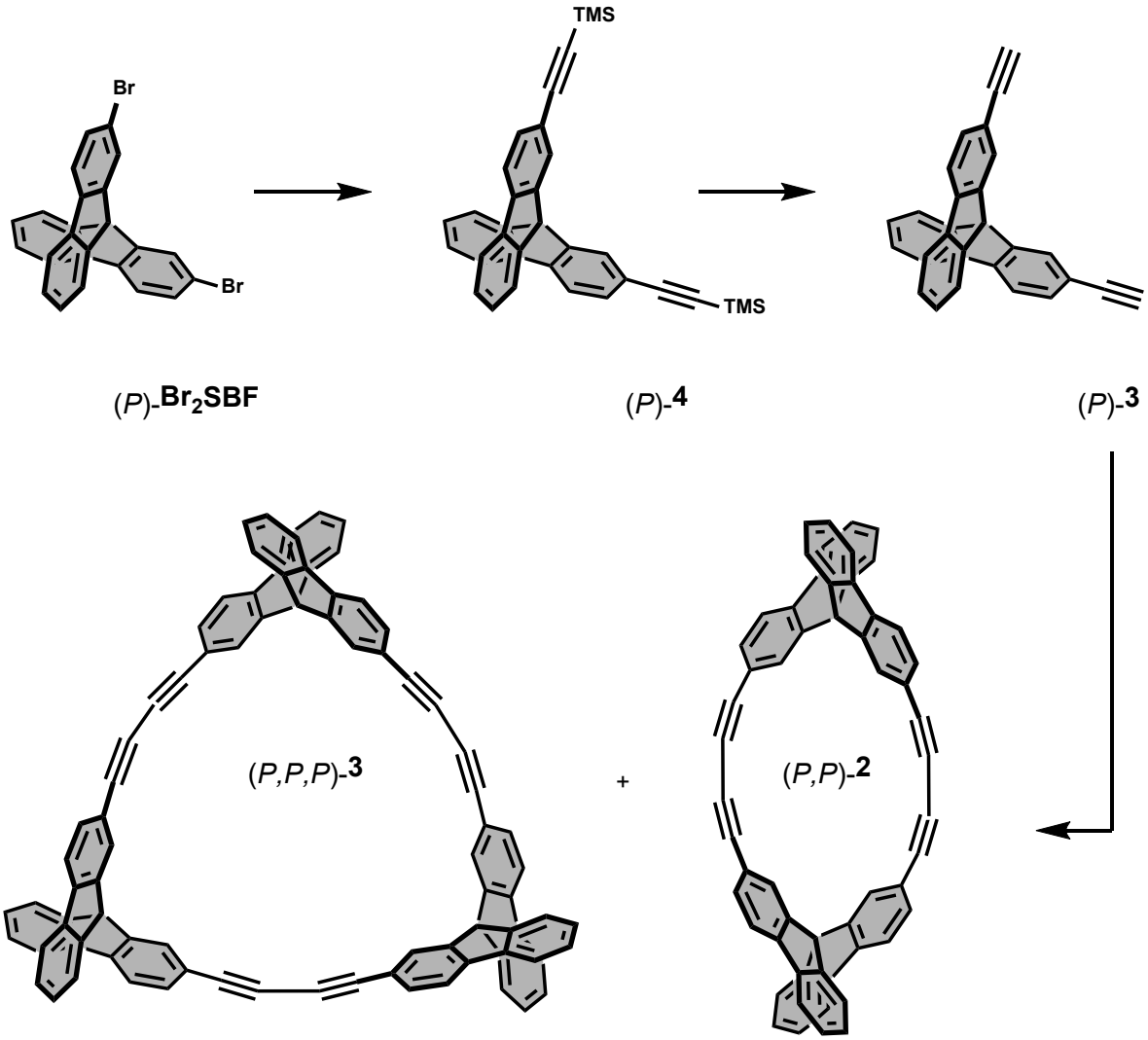

(*M*/*P*)-2,2'-Bis((trimethylsilyl)ethynyl)-9,9'-spirobi[fluorene] ((*M*/*P*)-4)

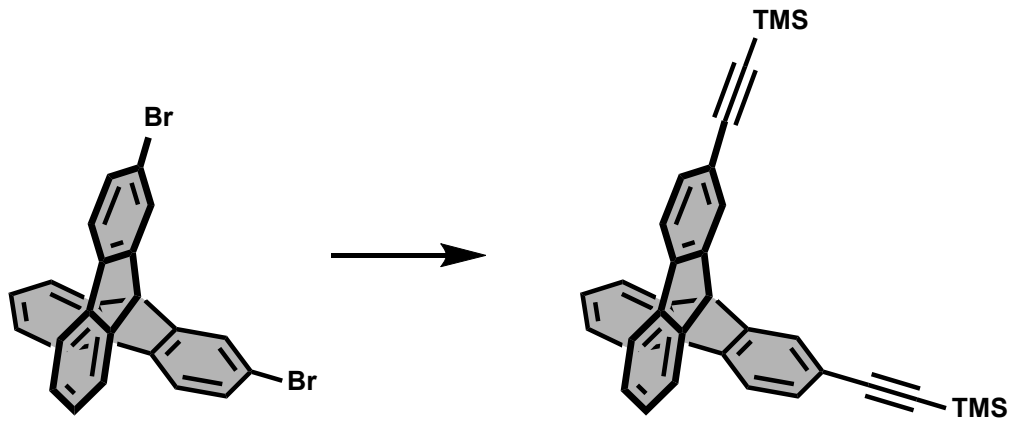

(*P*)-**Br$_2$SBF** (*P*)-**4**

(*M*/*P*)-**Br$_2$SBF** (1.1 mmol, 520 mg) and $Pd(PPh_3)_4$ (0.18 mmol, 208 mg) were dissolved in in 1,4-dioxane (11.5 mL) and Et_3N (6 mL) using a heat-gun flamed Schlenk tube under N_2 atmosphere. After degassing with three freeze-thaw-cycles, trimethylsilyl acetylene (6.99 mmol, 0.97 mL) was added and the resulting mixture was stirred for 22 h at 107 ºC. Once cooled down, the crude was purified by flash chromatography (SiO_2, gradient from 100% *n*-hexane to 3-10% EtOAc/n-hexane) to get (*M*/*P*)-**2** (555.8 mg, 98%), as a brown oil.

(*M*/*P*)-2,2'-Diethynyl-9,9'-spirobi[fluorene] ((*M*/*P*)-3)

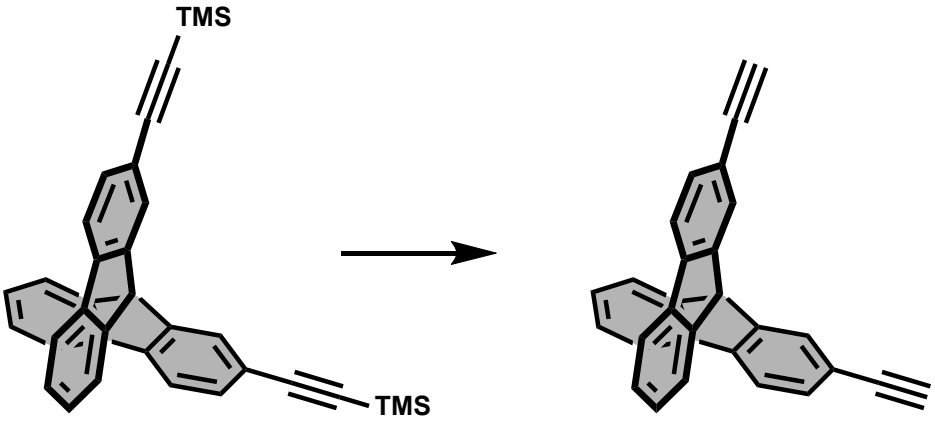

(*P*)-**4** (*P*)-**3**

(*M/P*)-**2** (1.09 mmol, 555.8 mg) was dissolved in a MeOH/THF (1:1) solution (20 mL). After that, K_2CO_3 (0.86 mmol, 119 mg) was added to the main mixture and stirred for 4 h at 25 ºC under air. The reaction was quenched with HCl(aq) 1M (4.97 mmol) and extracted with EtOAc (3x). The organic phase was washed with deionized H_2O (2x) and NaCl saturated solution (1x), and finally dried over anhydrous Na_2SO_4. As a result, (*M*/*P*)-**3** (398.8 mg, 80%) was obtained as a dark yellow solid.

Cyclo-tris-(2,2'-diethynyl-9,9'-spirobifluorene) ((*M*,*M*,*M*)-1/(*P*,*P*,*P*)-1)

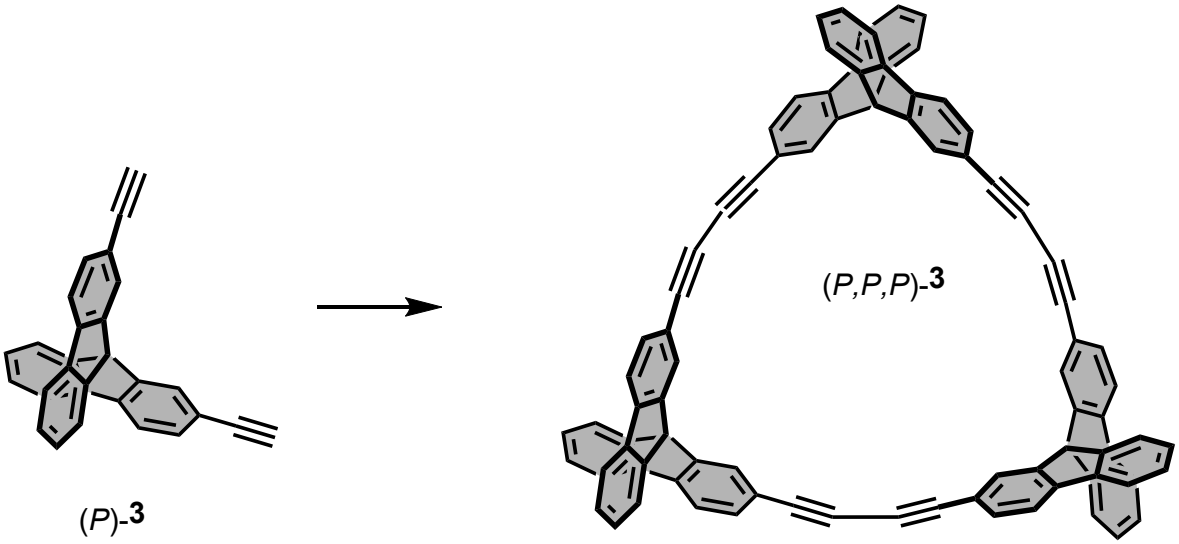

For this reaction two solutions were prepared. [$Pd(PPh_3)Cl_2$] (0.054 mmol, 38.2 mg), CuI (0.056 mmol, 10.64 mg), TMEDA (3.63 mmol, 0.54 mL) and toluene were added (Solution A) into a two-necked round-bottom flask, For solution B, (*M*)**-3** (0.22 mmol, 80 mg) is dissolved in toluene (20 mL) in a round-bottom flask. The solution B was added to solution A via a syringe performing a slow addition reaction for 15 hours at 100 ºC. Once cooled down, the crude was purified via flash column chromatography (SiO_2, gradient from 20% DCM/n-hexane to 50% DCM/n-hexane) yielded the enantiomeric compound (*M*,*M*,*M*)**-1** as a yellow solid (12.9 mg, 15%). Enantiomer (*P*,*P*,*P*)**-1** was analogously obtained from (*P*)**-3**.

Cyclo-bis-(2,2'-diethynyl-9,9'-spirobifluorene) ((*M*,*M*)-2/(*P*,*P*)-2)

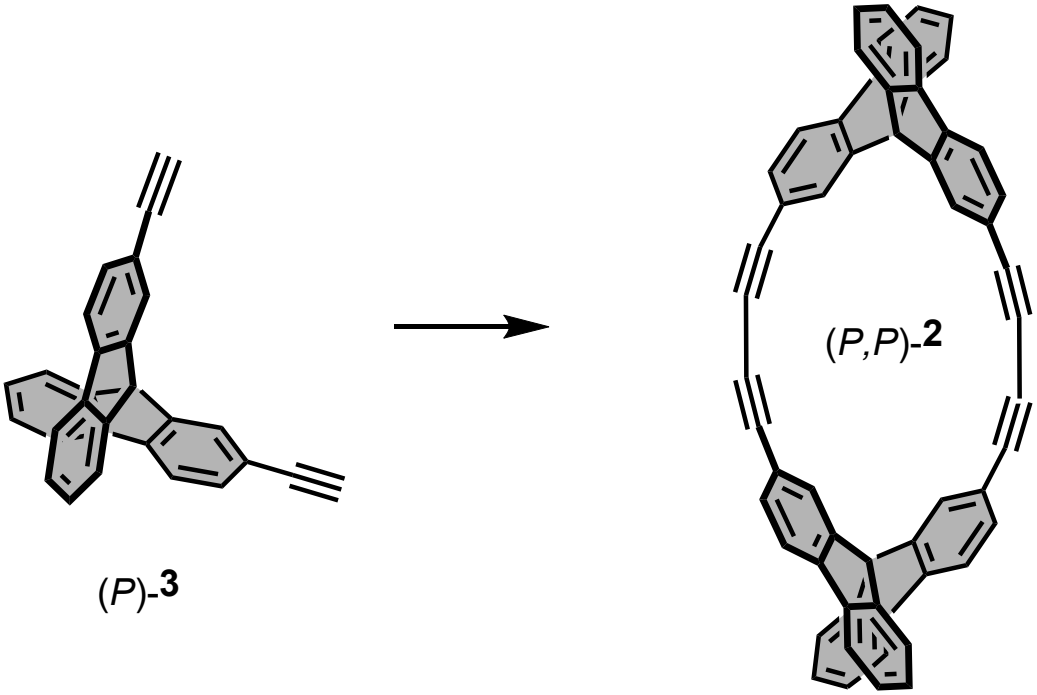

(*P*)-**3**

The procedure is similar to the ones for preparing ((*M,M,M*)-**1** and (*P,P,P*)-**1**) but reducing the temperature and reagents addition rate. Through this reaction the enantiomeric compound (*M,M*)-**2** (15 mg, 19%) was obtained as a yellow solid. Enantiomer (*P,P*)-**2** was produced starting from or (P)-**3**.

Section 2:

Electrocatalysis Oxygen Evolution Reaction (OER) Measurements

Ni felt Surface Activation

To study the SBFs as chiral additives for boosting the OER, the Ni felt electrode surfaces must be activated in alkaline media. Cyclic Voltammetry (CV) was used to activate them through the formation of a $Ni(OH)_x$ layer. Under these conditions, the soft ferromagnetic nature of nickel, the absence of an external magnetic field, and the limited range of spin-polarization effects collectively preclude any significant Ni magnetization on the active catalyst surface. The CVs were performed until the resulting CV curves show stable features. To verify that the surface was activated, Linear Sweep Voltammetry (LSV) was performed and the increase in current density due to the activation is visualized. Voltage (V_{RHE}) values are measured *vs.* a reference hydrogen electrode (RHE).

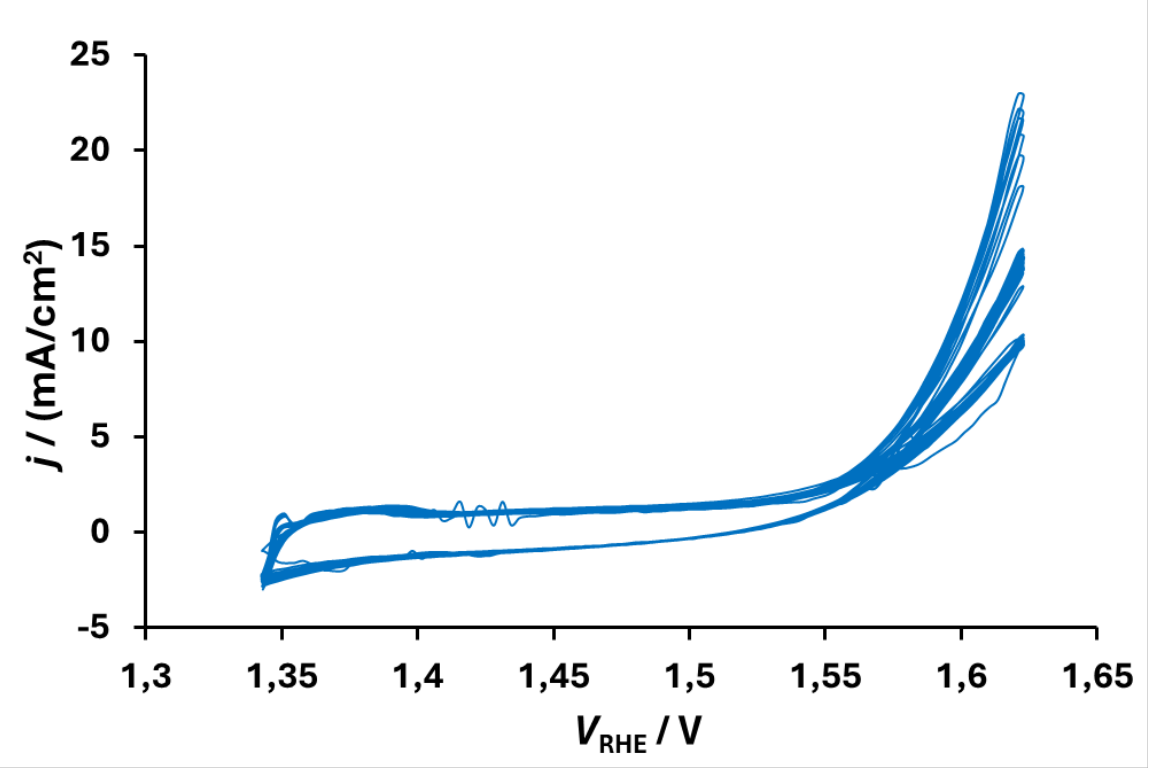

Figure S2: Cyclic voltammograms (50 mV/s) to activate Ni felt surface.

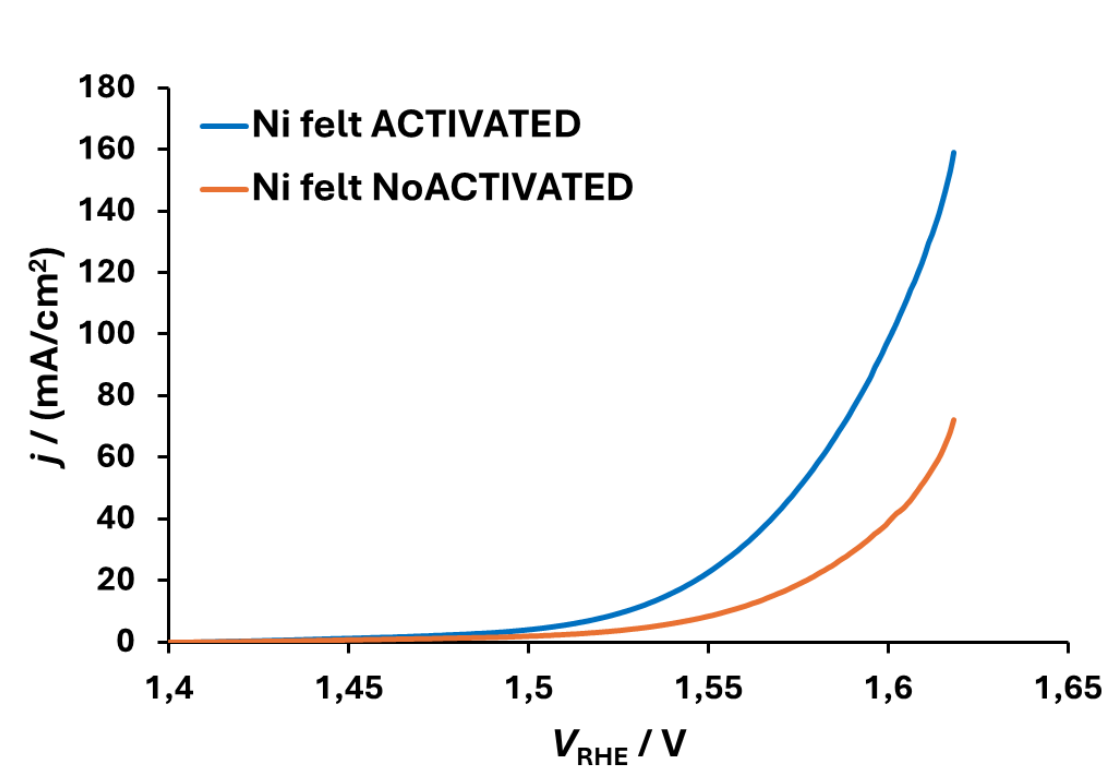

Figure S3: LSV curves before and after the surface activation through CV with 5 mV/s.

Loading Study on the Electrode Surface

Before the activation of the surface, an optimization of the loading parameters was carried out. LSV was performed using (*P,P,P*)-**1** and (*P,P*)-**2**, with loading of up to 0.8 mg/cm^2 to optimize loading yield. To check reproducibility, two identical electrodes were prepared with the same preparation method for each loading and compound. For both compounds the best loading was 0.1 mg/cm^2.

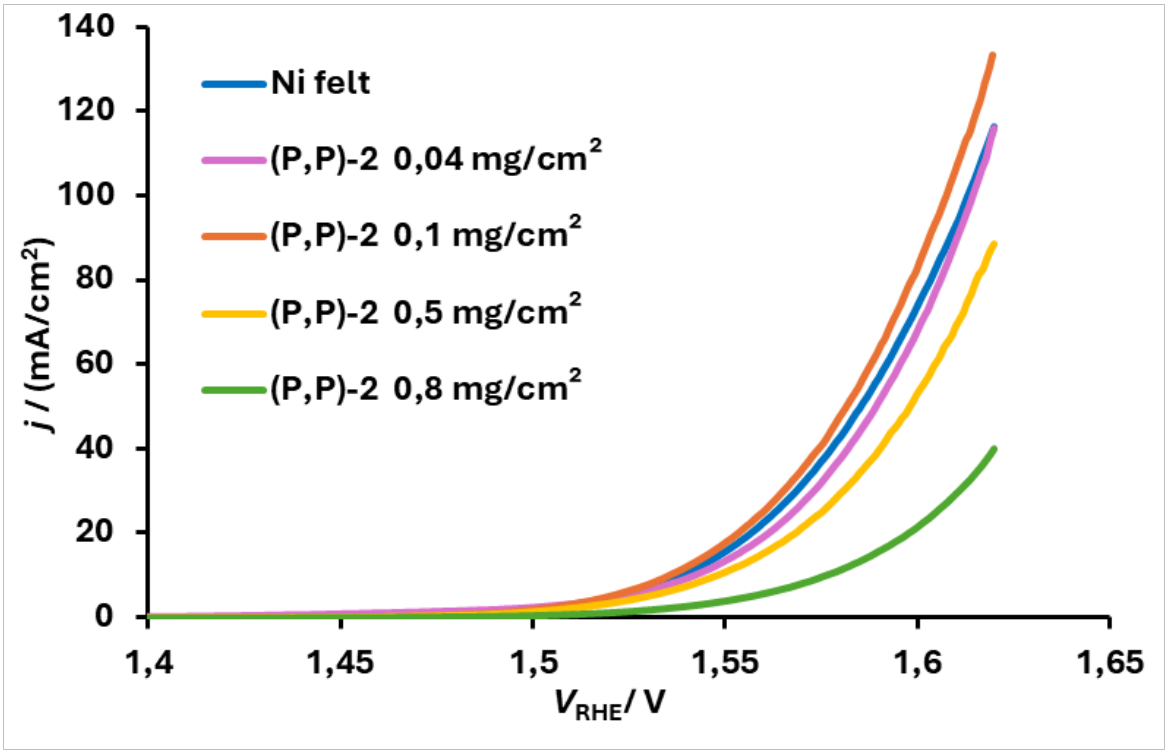

Figure S4: Loading study for the (*P,P*)-**2**. The LSV were performed at 5 mV/s.

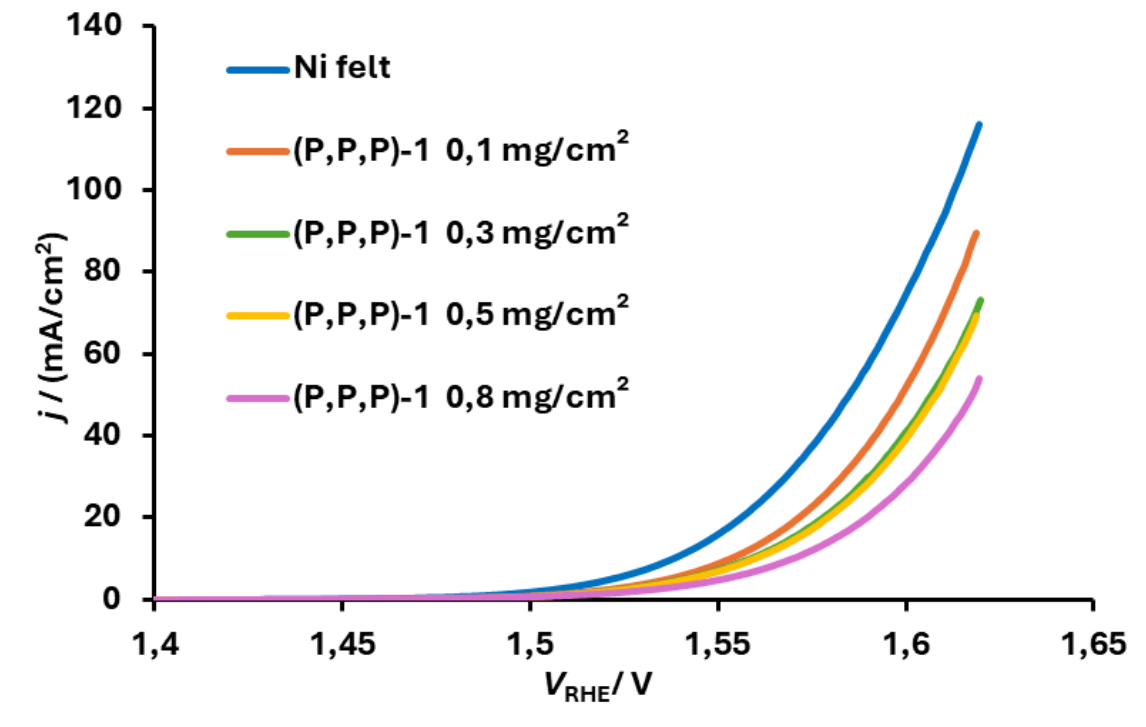

Figure S5: Loading study for (*P,P,P*)-**1**. The LSV were performed at 5 mV/s.

Double Layer Capacitance (C_{dl}) calculation

To determine the C_{dl}, a series of CV scans were performed at different scan rates (from 5 mV/s to 100 mV/s) within a narrow potential range *vs.* RHE (1.04 V to 1.14 V), in which faradaic processes should not occur. From the measurements, a linear relationship is obtained when plotting the capacitive currents ($\Delta j = j_{anodic} - j_{cathodic}$) against the scan rate, C_{dl} being 50% of the resulting slope.

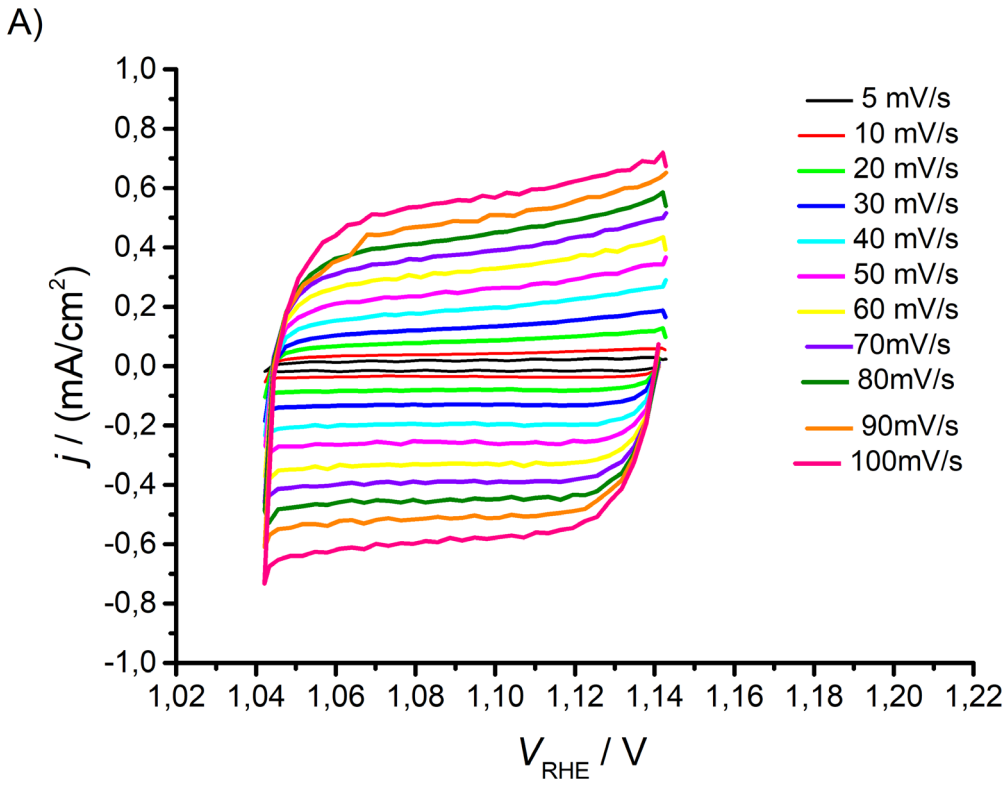

Figure S6: C_{dl} calculation for Ni felt.

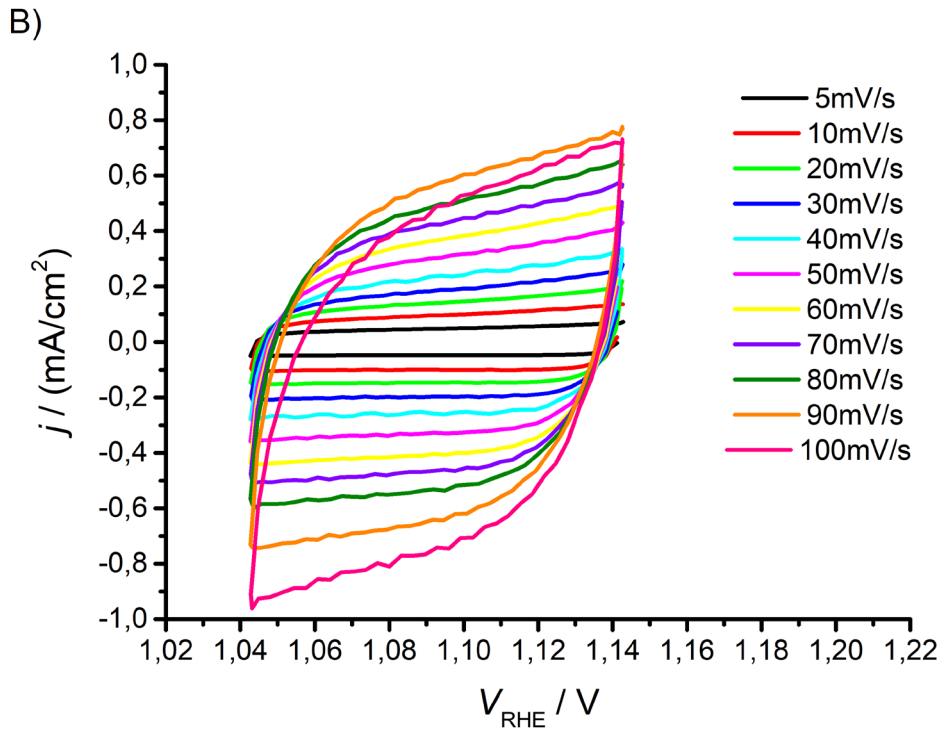

Figure S7: C_{dl} calculation for: (*P*)-**3**.

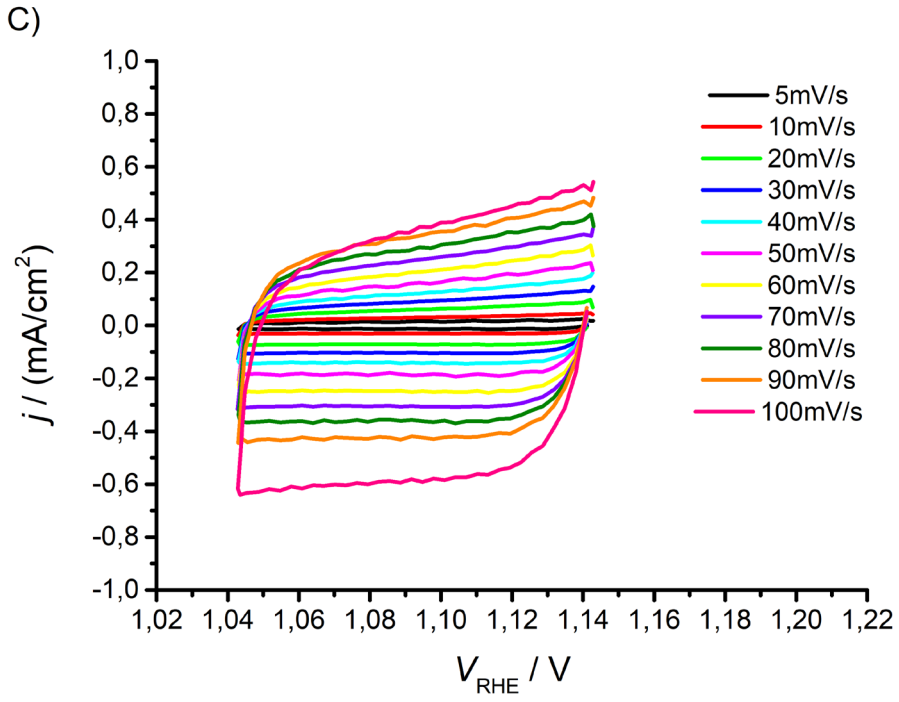

Figure S8: C_{dl} calculation for: (*P,P*)-**2**.

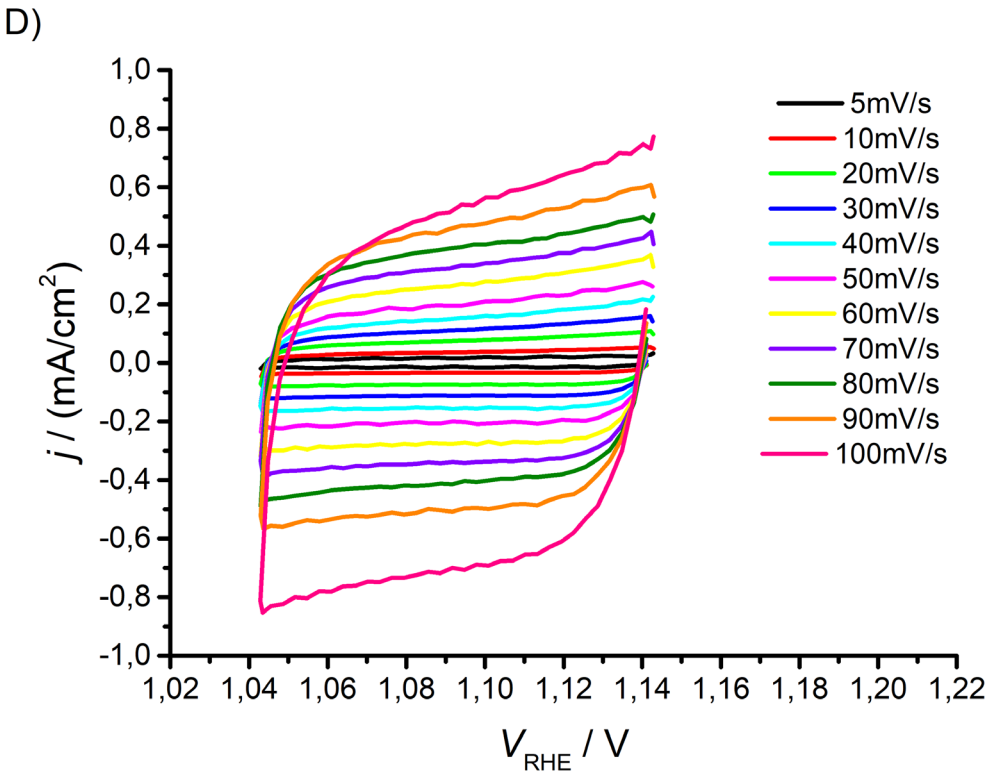

Figure S9: C_{dl} calculation for (*P,P,P*)**-1**.

Spectroscopic Analyses of (*M*,*M*,*M*)-1, (*M*,*M*)-2, and (*M*)-3 by Absorption, Electronic Circular Dichroism (ECD), g-factor, and Raman

In this section the ECD, Absorption and *g*-factor spectra of the **1**,**2** and **3** analog systems in solution are presented.

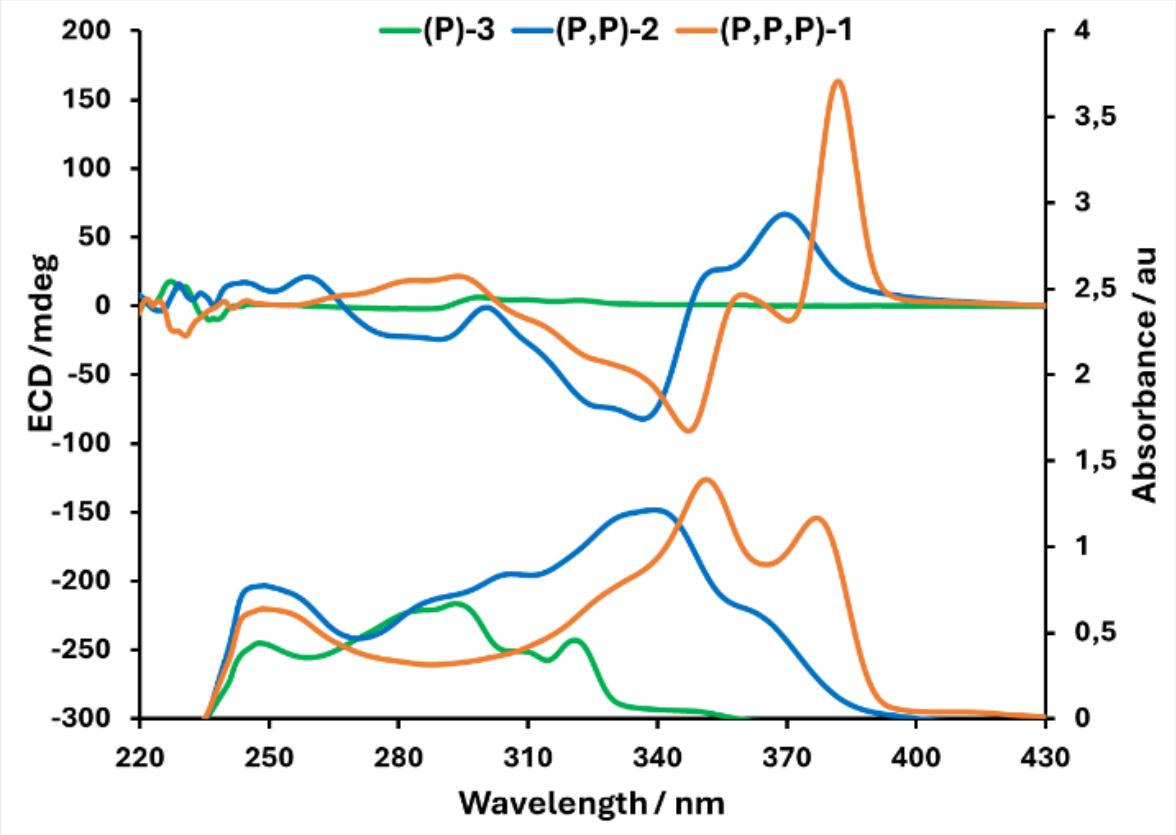

Figure S10: Experimental ECD and Absorption spectra for the three isomers with (*P*) configuration in chloroform (4×10^{-5} M).

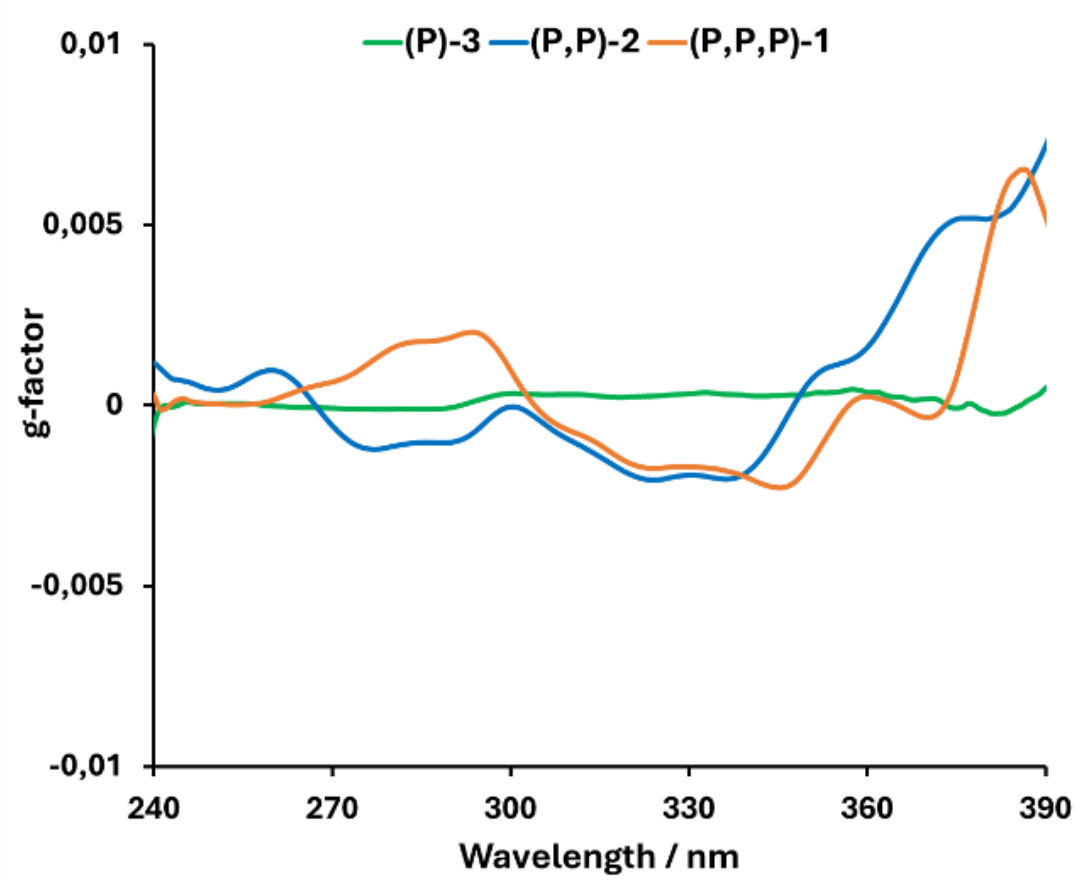

Figure S11: *g*-Factor for the three isomers with (*P*) configuration in chloroform (4×10^{-5} M).

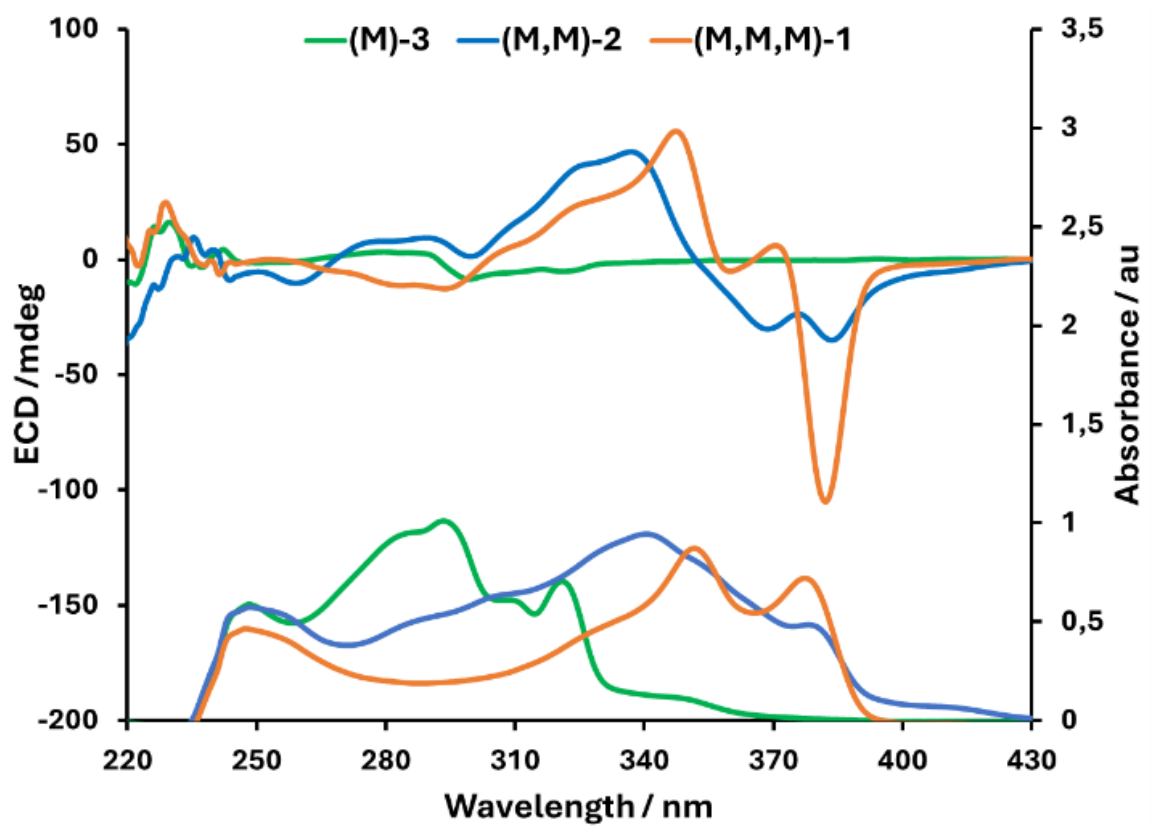

Figure S12: Experimental ECD and Absorption spectra for the three isomers with (*M*) configuration in chloroform (4×10^{-5} M).

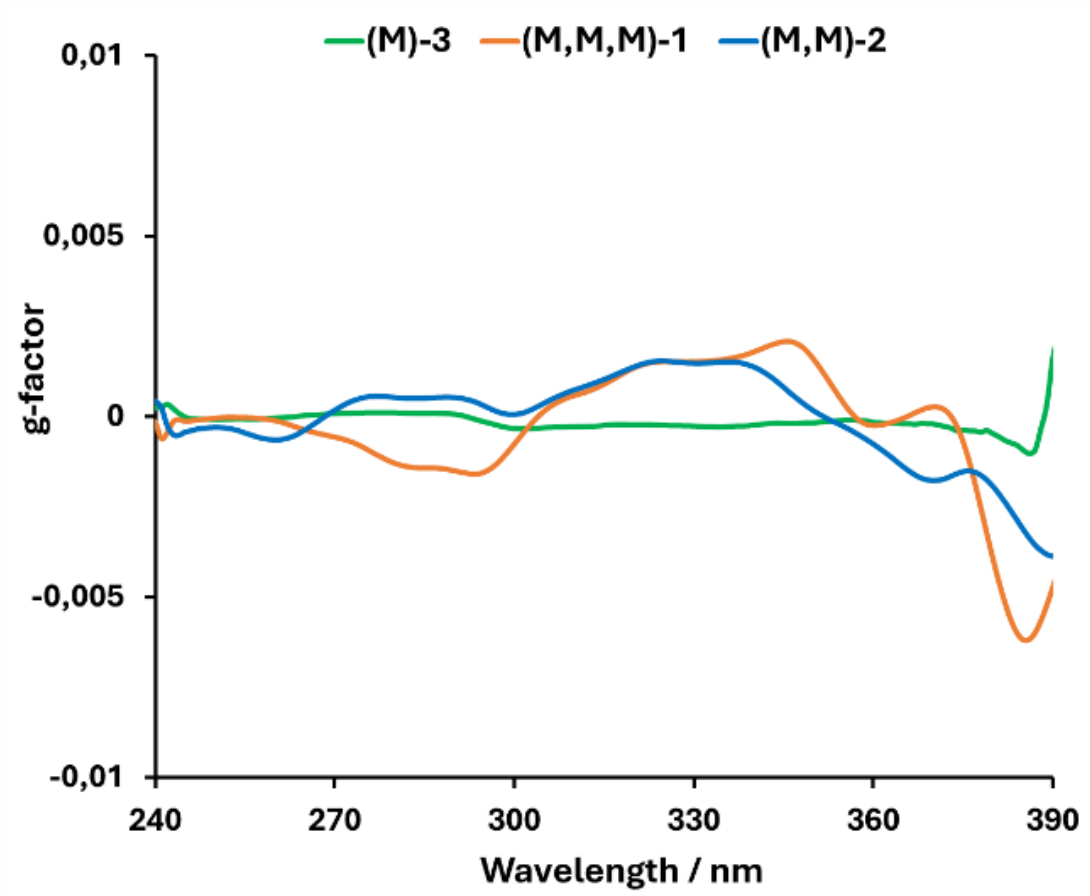

Figure S13: *g*-Factor for the three isomers with (*M*) configuration in chloroform (4×10^{-5} M).

On the other hand, to evaluate the effect of the OER on molecular stability, the ECD and Raman spectra of the compounds were analyzed before and after electrochemical treatment. For this purpose, two types of Ni felt electrodes were prepared for each enantiomer of compounds **3**, **2**, and **1**. The molecules were deposited on the electrodes using the drop-casting technique. One of the electrodes was then subjected to the OER process, while the other remained untreated, getting two types of samples: those not exposed to the electrocatalytic process (Pre-OER) and the exposed ones (Post-OER).

Raman spectroscopic measurements were performed on samples on compounds **3** and **2**. The equipment used was a Horiba Yobin Yvonne HR800 Raman Spectrometer. The measurements were performed with 633 nm laser emission wavelength using a 50X objective and 5 mW laser power to avoid changes of peak positions due to heating effects. To accurately verify the peak positions, an Oriel Pen 6032 (Ne) calibration lamp was used, and

the spectra calibrated with the 703.24 nm, 717.39 nm, and 724.52 nm Ne lines. The spectra of the analysed molecules evidenced sharp dominant peaks at 1607.5 cm^{-1} and 2206.3 cm^{-1} for (*P,P,P*)-**1**, and at 1607.5 cm^{-1} and 2212.0 cm^{-1} for (*P,P*)-**2**. The peaks at around 2210 cm^{-1} are attributed the C≡C stretching vibration of the acetylenes triple bonds that connect the SBF blocks, while the values at 1607 cm^{-1} can be assigned to the aromatic C=C bonds of the SBF blocks. Peak of Pre-OER and Post-OER positions were identical, indicating that the molecules are not significantly altered by the OER process, but the drop in intensity after OER suggests partial removal from the Ni-felt electrodes. The shift of the C≡C stretching vibration to lower wavenumbers for the (P,P,P)-**1** compared to (P,P)-**2** is consistent with a lengthening of the C≡C bond in the ring structure of PPP-**1**.

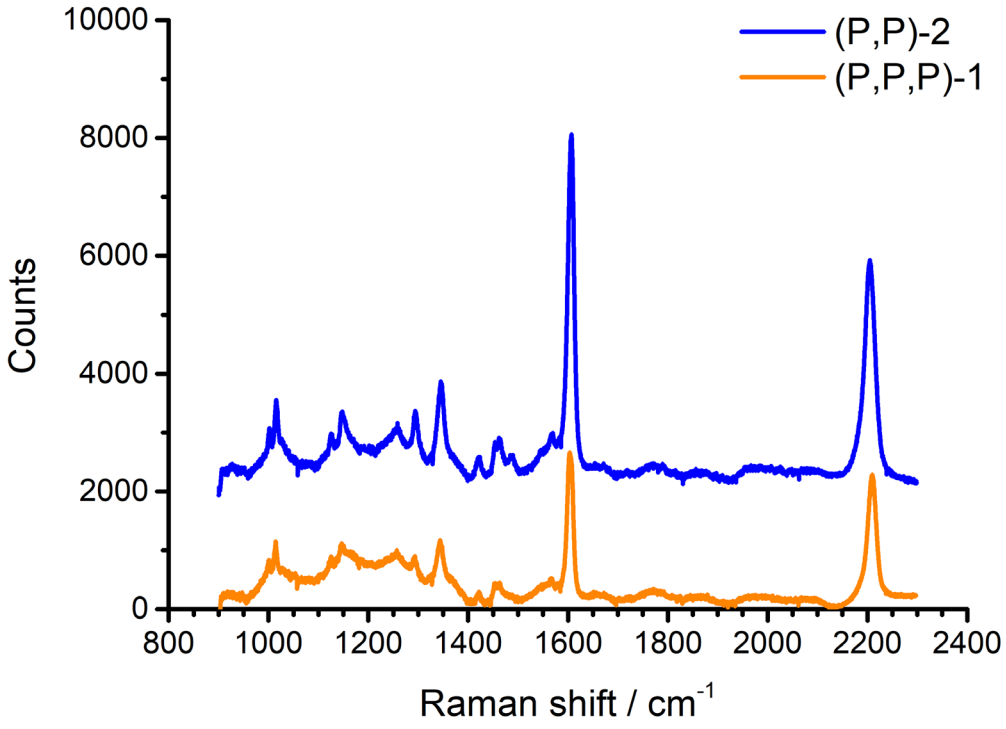

Figure S14: Raman spectra of (*P,P,P*)-**1** and (*P,P*)-**2** drop casted on Si(100).

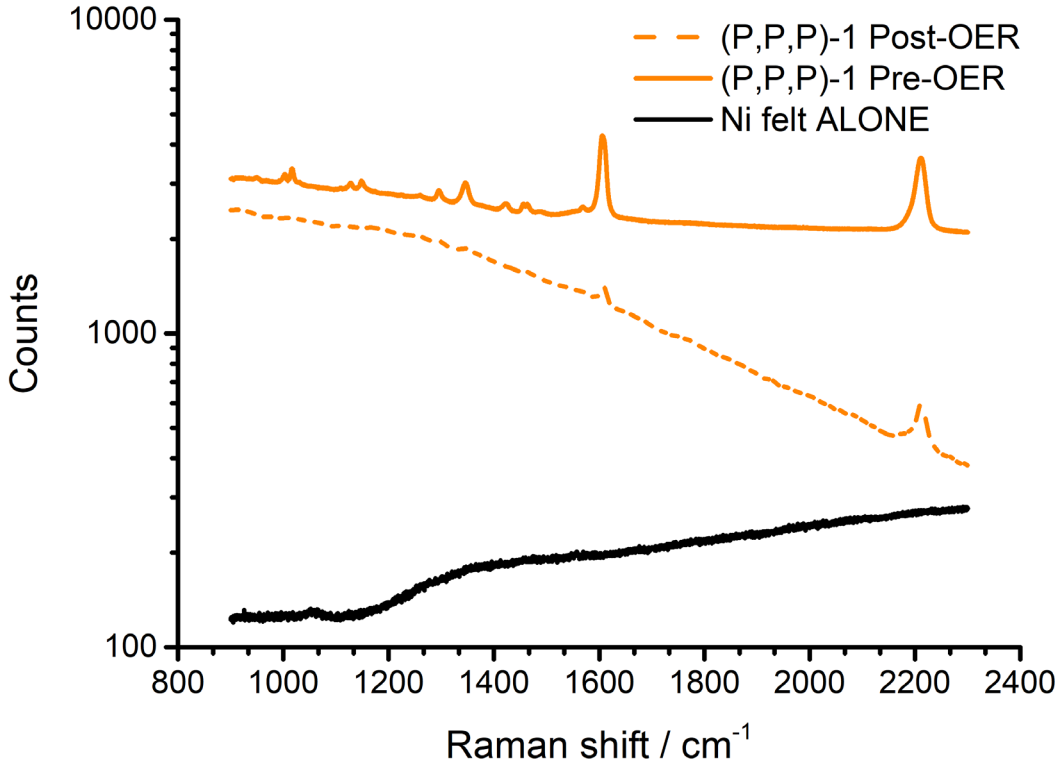

Figure S15: Raman spectra of (*P,P,P*)-**1** over Ni-felt before and after OER as well as the pure Ni felts alone.

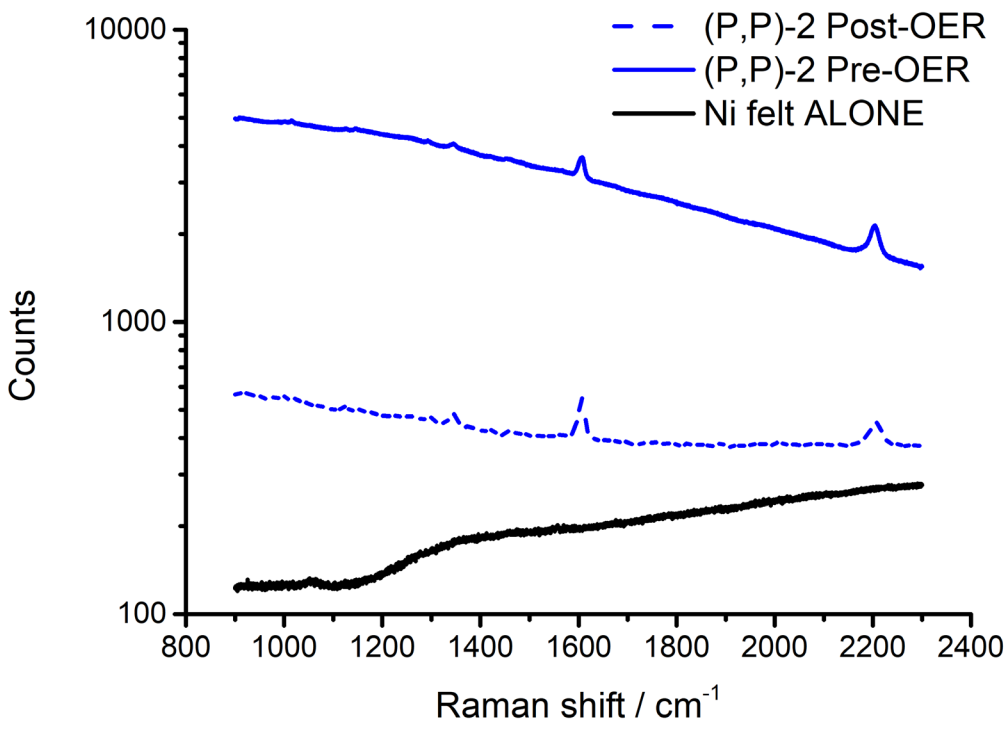

Figure S16: Raman spectra of (*P,P*)-**2** over Ni-felt before and after OER as well as the pure Ni felts alone.

After that, the electrodes were redissolved in 2 mL $CHCl_3$ and the ECD was measured to compare the differences between the spectra. The results for (*P,P*)**-2** and (*P*)**-3** were analogous to those shown in the manuscript for (*P,P,P*)**-1** with no significant differences between the samples before and after OER, confirming the stability of the molecules after OER.

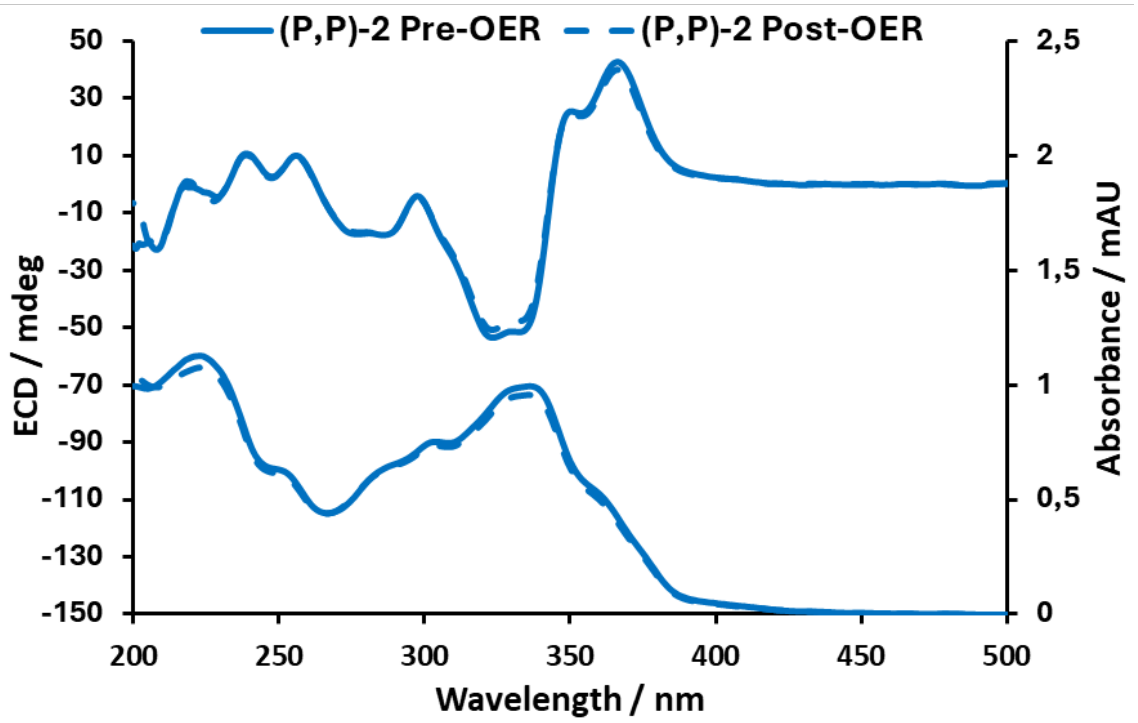

Figure S17: Electronic circular dichroism and UV–Vis absorption spectra of (*P*,*P*)-**2** before and after OER experiments.

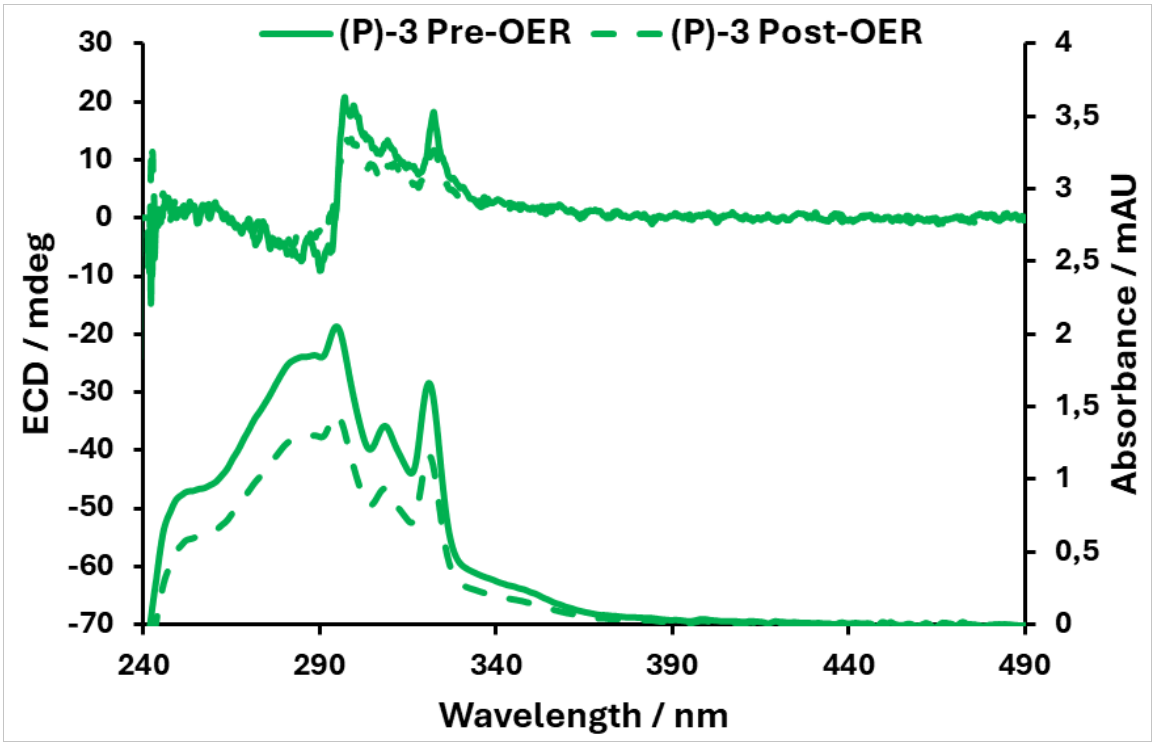

Figure S18: Electronic circular dichroism and UV–Vis absorption spectra of (*P*)-**3** before and after OER experiments.

Structure Validation by ^{1}H NMR spectroscopy

(*P,P,P*)/(*M,M,M*)-**1**

^{1}H NMR (400.16 MHz, $CDCl_3$, δ): 7.83 (d, J = 7.6 Hz, 6H), 7.77 (d, J = 8.0 Hz, 6H), 7.45 (d, J = 7.9 Hz, 6H), 7.39 (t, J = 7.4 Hz, 6H), 7.14 (t, J = 7.5 Hz, 6H), 6.85 (s,6H), 6.73 (d, J = 7.6 Hz, 6H) ppm.

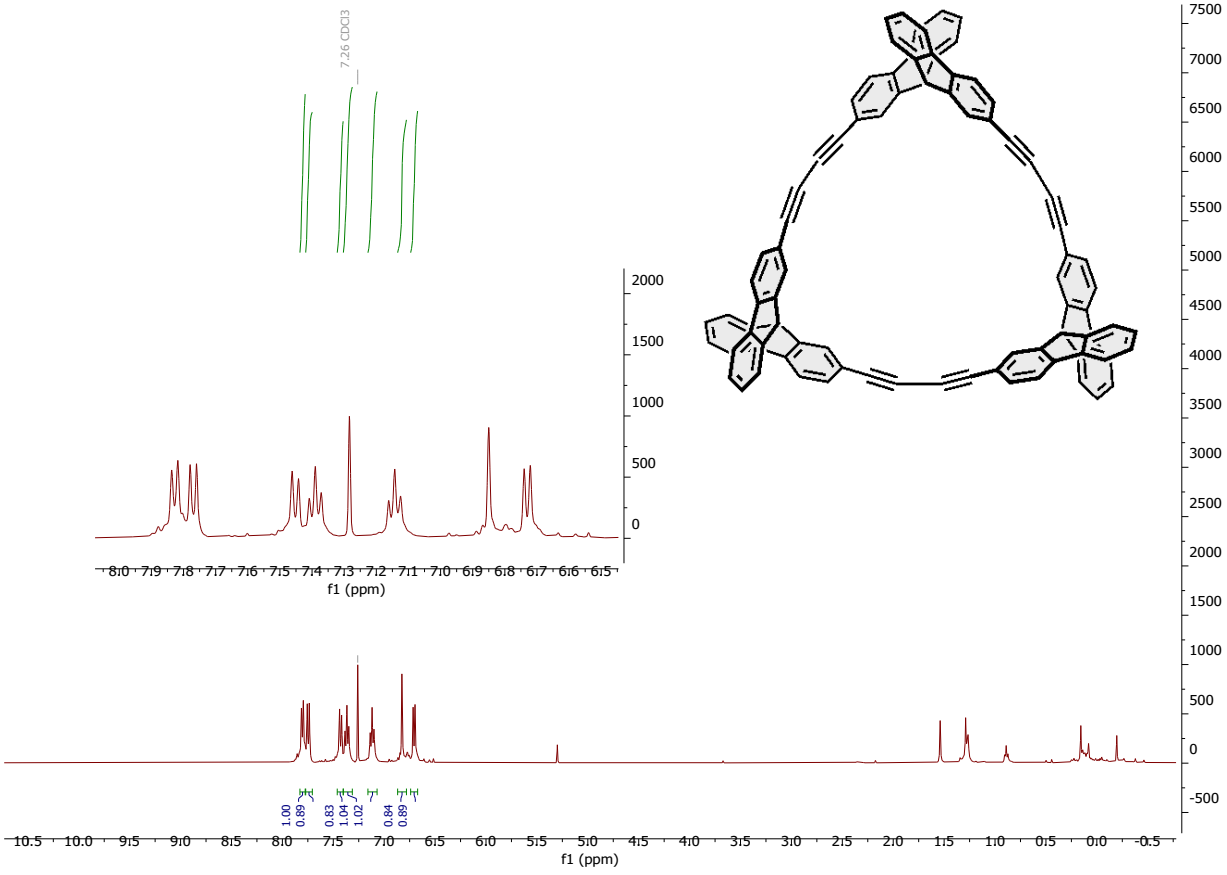

(*P,P*)/(*M,M*)**-2**

^{1}H NMR (400.16 MHz, CDl_3, δ): 7.80 (t, J=8.0 Hz, 8H), 7.47 (d, J=8.0 Hz, 4H), 7.35 (t, J=7.5 Hz, 4H), 7.11(t, J=7.4 Hz, 4H), 6.61 (d, J=7.7 Hz, 4H)

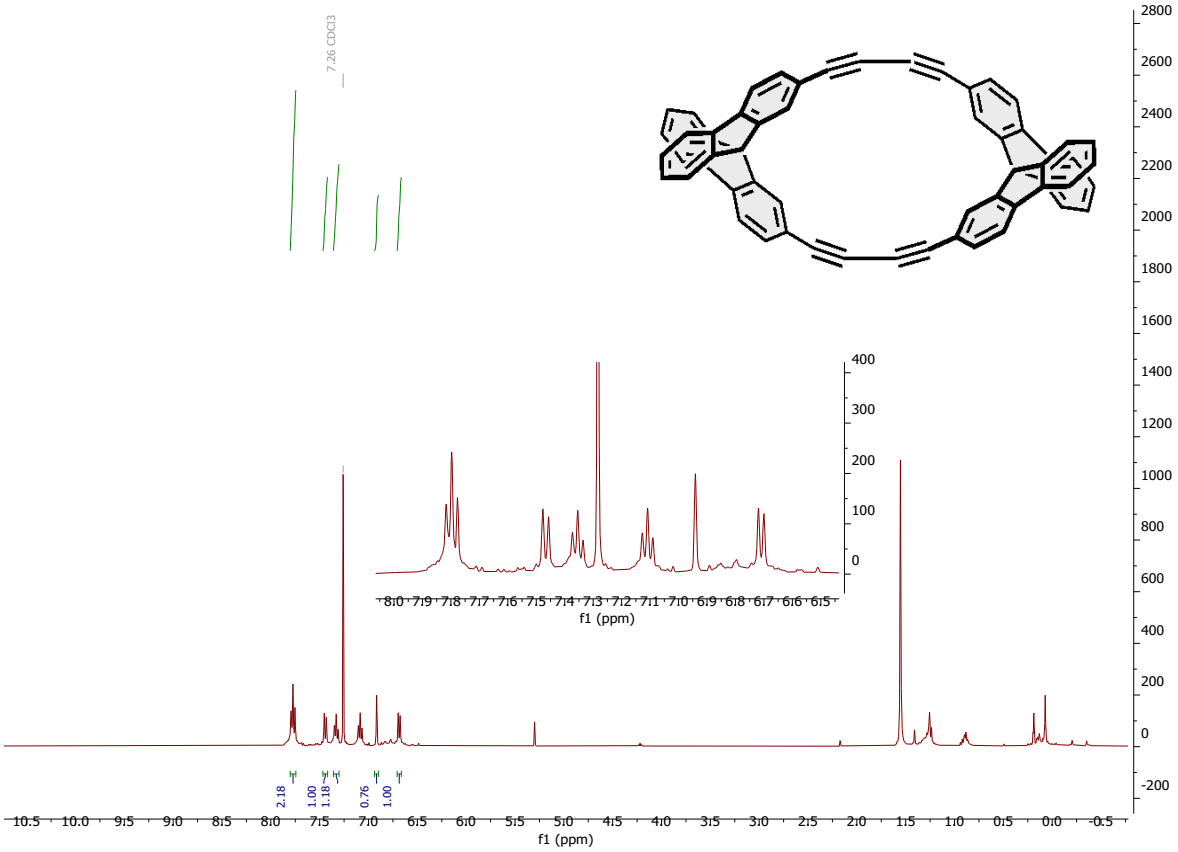

(*P*)/(*M*)-**3**

^{1}H NMR (400 MHz, $CDCl_3$) δ 7.85 (dt, J= 7.7, 1.2 Hz, 2H), 7.81 (dd, J = 7.9, 0.7 Hz, 2H), 7.54 (dd, J = 7.9, 1.5 Hz, 2H), 7.41 (td, J = 7.5, 1.1 Hz, 2H), 7.16 (td, J = 7.5, 1.1 Hz, 2H), 6.86 (dd, J = 1.5, 0.7 Hz, 2H), 6.75 (dt, J = 7.6, 0.9 Hz, 2H), 3.00 (s, 2H).

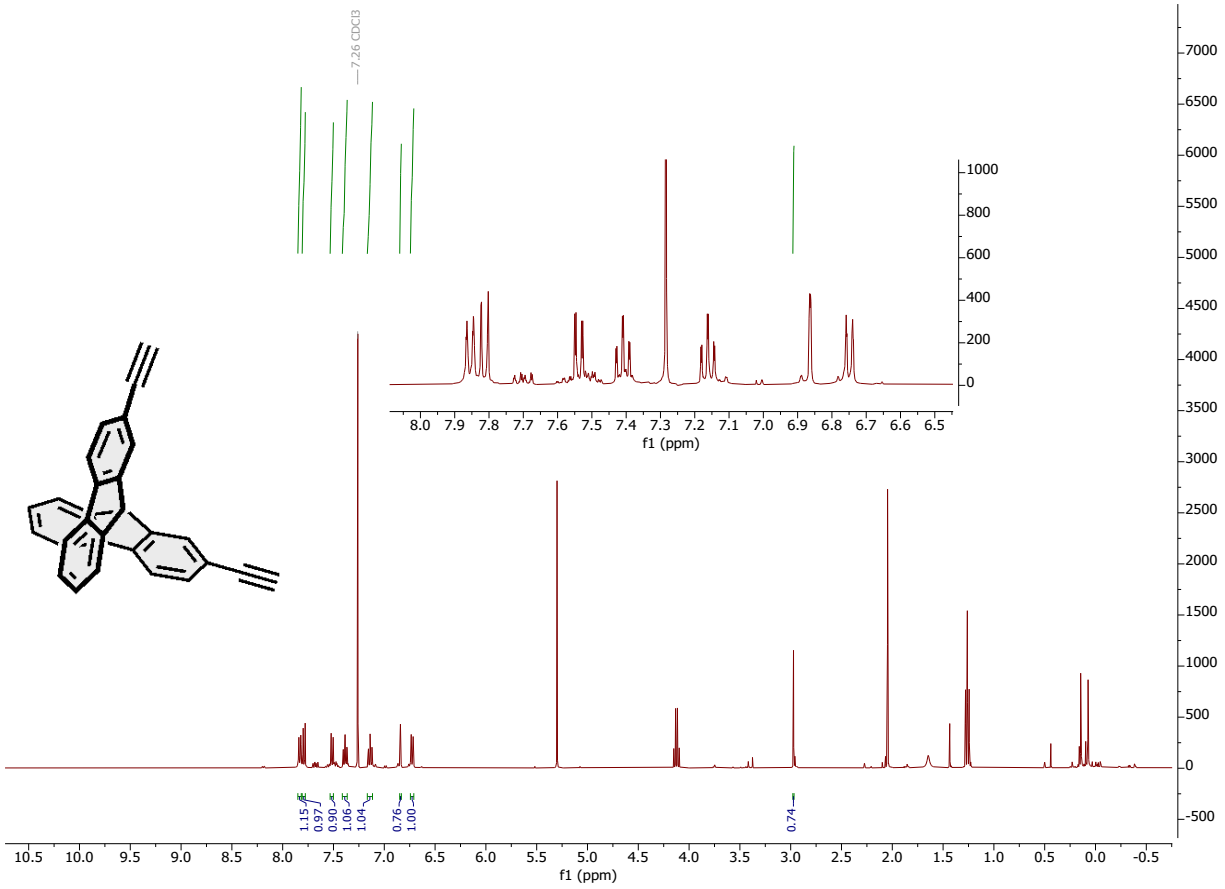

References

[1] S. Castro-Fernández, R. Yang, A. P. García, I. L. Garzón, H. Xu, A. G. Petrovic, J. L. Alonso-Gómez, *Chem. Eur. J.* , **2017**, *23*, 11747–11751

[2] A. Ozcelik, D. Aranda, S. Gil-Guerrero, X. A. Pola-Otero, M. Talavera, L. Wang, S. K. Behera, J. Gierschner, Á. Peña-Gallego, F. Santoro, R. Pereira-Cameselle, J. L. Alonso-Gómez, *Chem. Eur. J.*, **2020**, *26*, 17342–17349